Available online at www.sciencedirect.com

ScienceDirect

Procedia Structural Integrity 2 (2016) 3135–3142

Structural Integrity Procedia

www.elsevier.com/locate/procedia

21st European Conference on Fracture, ECF21, 20-24 June 2016, Catania, Italy

On effect of pre-bending process on low cycle fatigue behaviour of high strength steel using lock-in thermography

Reza H. Talemi[a,*], Saosometh Chhith[b], Wim De Waele[b]

[a]*ArcelorMittal Global R&D Gent-OCAS N.V., Pres. J.F. Kennedylaan 3, 9060 Zelzate, Belgium*
[b]*Soete Laboratory, Ghent University, Technologiepark Zwijnaarde 903, 9052 Zwijnaarde, Belgium*

Abstract

The application of High Strength Steel (HSS) on different structural components is becoming more attractive. They have a fine grain structure, low carbon content for improved weldability, and controlled internal purity. These steel grades are frequently used for structural applications. There are a lot of steel components of the considered applications that are subjected to bending and fatigue loading conditions, respectively. It is well known that under critical loading conditions, cyclic stress, which exceeds the material yield stress, can occur at some critical locations such as the inner side of bent components. Combining these two aspects, i.e. the bending process followed by fatigue loading, causes multiple micro-crack initiation inside the inner surface of the bending area, which is followed by propagation of the cracks up to final rupture of material.

The main objective of the present study is to investigate the effect of pre-bending process of HSS subjected to low cycle fatigue loading conditions, since so far only very limited amount of research has been focused in this direction. For this purpose, in the first step, a new test set-up was designed to take into account the effect of pre-bending process when the fatigue load has been applied. Lock-in thermography technique was used to monitor the incremental temperature variation during fatigue cycling at the bending root. Using the temperature evolution, the crack initiation and propagation lifetimes were separated from total lifetime. Fractography and Scanning Electron Microscopy (SEM) analyses were performed to study the fracture surface of specimens after bending and fatigue testing. Furthermore, numerical technique approach was used to model the bending and spring back processes along with the fatigue loading in order to understand the effect of bending process on fatigue behaviour of tested material. The developed finite element model provides more information about the multiaxial strain and stress states at and near the bending root after bending process and applied axial fatigue load.

Peer-review under responsibility of the Scientific Committee of ECF21.

Keywords: Bending process; Low cycle fatigue; Lock-in thermography; Numerical modelling

1. Introduction

The HSS grades combine outstanding mechanical properties (very high strength, fatigue resistance and toughness) with good formability and weldability. The guaranteed high yield strength of these grades makes it possible to achieve substantial weight reduction through thickness reduction, whilst maintaining overall performance and safety. These

* Corresponding author. Tel.: +32-9 345 12 82; fax: +32-9 245 75 12.
E-mail address: Reza.HojjtaiTalemi@arcelormittal.com

Peer review under responsibility of the Scientific Committee of ECF21.
10.1016/j.prostr.2016.06.391

steel grades are therefore frequently used to replace structural steel grades where weight reduction is required. Thickness reduction brings additional savings when processing the material, since it is easier to weld, and reduces transport costs.

Their very high yield strength contributes to a solution that increases the payload capacity and gives higher strength structures. Typical applications include telescopic cranes, tippers, truck and trailer manufacturing industries, where the emphasis is on strength and weight reduction potential. However, in spite of their great advantages of the high yield strength, the use of these steels faces some important challenges. In general, fatigue performance of high strength steels is less investigated compared with construction mild steels. However, this topic has been gaining much interest in the last decade, Chen et al. (2007). The fatigue life of components can be determined in terms of stress, Wohler (18711), strain, Basquin (1910), or dissipated energy parameters, Coffin (1953).

There are a lot of steel components of above mentioned applications that are subjected to bending and fatigue loading conditions respectively. Combining these two aspects i.e. bending and fatigue causes a premature micro-crack initiation inside the inner surface of bent region and propagation of the cracks up to final rupture of material. The bending process might represent a weak point and induce micro-crack like defect at bending root. These micro defects act as a high stress concentration site. Accordingly, some fatigue cracks have been detected in the structures within a few years of their service life, and cannot be properly explained using available standard high and low cycle fatigue approaches in the literature by Beretta et al. (2009). Crupi et al. (2010) have used infrared thermography to investigate the low cycle fatigue of base metals and welded joints. They have successfully correlated the thermal increments during the fatigue test to the hysteresis loops derived from the traditional procedure. They have shown that there is a correlation between the stable hysteresis loops and the stabilized temperature.

The main objective of the present study is to investigate the effect of pre-bending process of HSS subjected to Low Cycle Fatigue (LCF) loading conditions, since so far only very limited amount of research has been focused in this direction. In the first step, it was tried to understand the low cycle fatigue behaviour of HSS in terms of fatigue crack initiation and propagation lifetime. Therefore, an advanced lock-in infrared thermography approach was used to separate crack initiation and propagation lifetimes. Fractography and Scanning Electron Microscopy (SEM) analyses were performed to study the fracture surface of the failed fatigue specimens after the bending process and the fatigue testing. Furthermore, a three dimensional finite element modelling approach was used to simulate the bending process and fatigue loading conditions. The developed model allows to monitor the multiaxial stress and strain states inside the bending area.

2. Material

In this study S700MC steel grade was used to investigate the effect of pre-bending process on its LCF behaviour. S700MC material is a thermo-mechanically, hot rolled material which is suitable for cold forming. Moreover, S700MC has a fine grain structure, a low carbon content for improved weldability and controlled internal purity. All samples were received in 8mm thickness, after levelling. In order to verify the actual static strength properties of the material used in this investigation, three quasi-static monotonic tensile tests were performed. Average yield stress and tensile strength of 841MPa and 885MPa were obtained, respectively.

3. Experiments

3.1. Test set-up

As mentioned above the main objective of this study is to investigate the effect of pre-bending process on the LCF performance of high strength steel. To this end, a new experimental set-up has been developed. Specimens of 320mm long and 80mm wide were taken from a sheet, with a reduced width of 64mm at centre of specimen. The longest side of the specimen was perpendicular to the rolling direction (RD). The initial geometry of the fatigue sample was according to recommendations provided by ASTM E606 standard, although, the width of bent sample was increased in order to have plain strain condition in the middle of specimen after bending process as illustrated in Fig. 1(a). All samples were bent 90° using a tool radius of two times the sheet thickness, i.e. 16mm. Springback effects were compensated so as to obtain a final angle as close as possible to 90° ± 1. In order to apply axial fatigue load to the

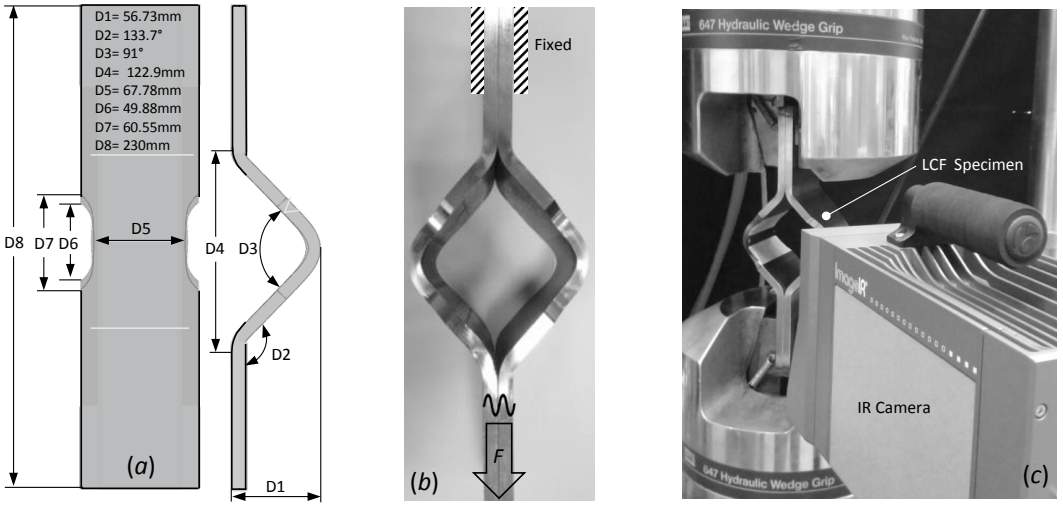

Fig. 1. (a) schematic illustration of fatigue specimen after 90° bending with bending ratio i.e. r/t=2; (b) the LCF specimen after welding along with the applied fatigue boundary and loading conditions; (c) the LCF fatigue set-up and location of IR camera. The IR camera was focused on area of interest, which is the bending root.

specimen and avoiding any secondary bending moment on grippers, after bending, two identical samples were welded together to obtain a symmetrical configuration. Fig. 1(b) demonstrates the final geometry of the bent fatigue specimen after applying the bending process. All specimens had proper edge preparation, i.e. all burrs were removed, so as to avoid crack initiation from the edges during fatigue testing. Fig. 1(c) depicts the LCF fatigue experimental set-up used in this study.

The fatigue tests were performed on a hydraulic testing machine as shown in Fig. 1(c). Force-controlled experiments were carried out using six different axial load (stress) levels from 25 to 70kN to produce the S-N curve. The fatigue loads were applied with 0.1 loading ratio at frequency of 2Hz. At least two fatigue tests were performed at each load (stress) level for checking repeatability of results.

3.2. S-N curve and fractography

Fig. 2 (a) shows the applied stress versus total number cycles to final fracture. The test was stopped when the displacement value reached +1mm above the stabilisation point, which was considered as the final failure. All specimens showed cracks at the bending root. To calculate the stress levels, the applied axial loads were divided over the narrowest net section of the bent fatigue sample i.e. 2 × 64mm × 8mm (Fig. 1(a)). As mentioned, the onset of crack initiation was considered at 0.1mm displacement at constant applied load during the fatigue cycling.

From the displacement variation it was not possible to estimate the crack length at 0.1mm displacement at presence of constant applied axial load. To investigate this more into the details, for case of F= 40kN, the test was stopped at 0.1mm displacement. There was no evidence of cracking after visual inspection. Therefore, a fractography analysis was done to find the crack length associated to 0.1mm displacement. The fatigue sample was cross sectioned in the middle of the bending area perpendicular to the axial loading direction. The crack length then was measured using SEM after embedding the sample inside epoxy. Fig. 2(b) shows the SEM micrograph for the left side sample of the fatigue specimen. It can be noticed that the crack size was about 0.64mm length. This crack size can be considered as onset of the fatigue macro crack initiation. However, defining the initial crack size is not a straight forward procedure and depends on different parameters such as grain size, material properties and practical application and so on. Fig. 2(c) shows the fracture surface of a failed fatigue sample at F= 40kN. As indicated in the figure multiple fatigue cracks were initiated inside the bending area. These small cracks are joined to form a big crack up to final fracture of the fatigue specimen. It can be noticed from the figure that the fatigue crack propagates up to 3.5 mm length followed by a sudden tensile fracture.

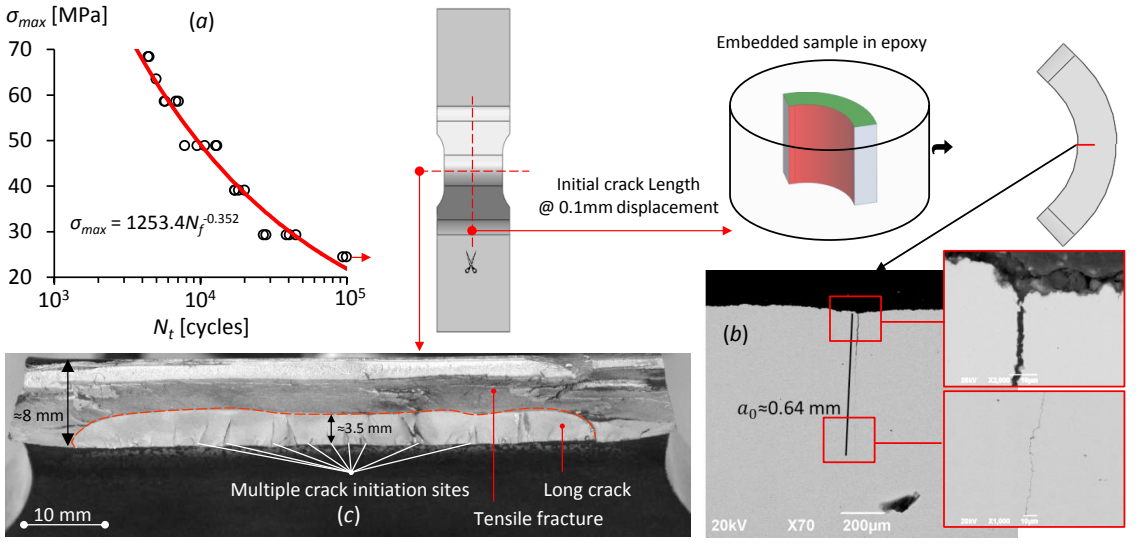

Fig. 2. (a) typical S-N curve for bent specimen under LCF loading conditions; (b) measured crack length at 0.1mm displacement at F=40 kN applied fatigue load; (c) fracture surface of failed fatigue sample at F=40 kN.

3.3. Lock-in thermography

In principle, thermography is a measurement technique which provides an image of the distribution of the temperature on the surface of an examined object. Thermal images are actually visual displays of the amount of infrared energy emitted, transmitted, and reflected by an object. The technique is called passive or classical if steady-state temperature contrast is imaged. On the other hand, it is called active thermography if the sample temperature is actively influenced by other means. Lock-in thermography, an active thermography, is currently widely used in non-destructive testing e.g. for thermo-mechanical applications (thermoelastic and thermoplastic investigations) and for mechanical fault detection based on periodic ultrasonic excitation.

The goal of this investigation was to detect a surface crack initiation by analysing temperature evolution of local heat sources on the sample surface. Therefore, continuous acquisition of thermal images is made at the frame rate of 20Hz from the start to the end of the fatigue test under controlled room temperature. In this way, the number of images per fatigue cycle is 10, which can be considered as oversampling for accuracy of the data processing. Without applying any secondary heat sources, the temperature evolution during fatigue processes mainly results from three effects: thermoelastic effect, inelastic effect (irreversible heat dissipation) and environmental heat transfer effect. Since this temperature is modulated by a periodic sinusoidal fatigue load, it can be estimated by

$$T_{exp}(t) = T_0 + \Delta T.t + T_1 sin(\omega t + \varphi_1) + T_2 sin(2\omega t + \varphi_2) \quad (1)$$

Where, T_{exp} is overall experimental temperature, ω is the angular frequency of the fatigue loading, $T_0 + \Delta Tt, T_2 sin(\omega t + \varphi_2)$ are linear drift and second harmonic effect, respectively which accounts for the inelastic and the environmental heat transfer effects, and $T_1 sin(\omega t + \varphi_1)$ is first harmonic effect which accounts for purely thermoelasticity. The thermoelastic temperature amplitude can be determined as:

$$T_1 = -KT_0 (\sigma_1 + \sigma_2 + \sigma_3) \quad (2)$$

where T_1 is the material temperature, T_0 is room temperature, $K = \alpha/C_p \rho$, α is the coefficient of the linear-thermal expansion, ρ is the density, C_p is the heat capacity at a constant pressure, and σ_i (i= 1,3) is the principal stress. The minus sign on the right hand side of the equation justifies that tension gives a drop of the sample temperature while compression gives a rise of the sample temperature within elasticity of materials. Instead of analysing the overall temperature, the simpler parameter, the thermoelastic temperature amplitude T_1, can be used as indicator for crack initiation due to its relation with stresses. This temperature amplitude can be extracted from the measured overall

experimental temperature by applying the standard lock-in correlation. Krapez (1998) has introduced an approach which relies on the multiplication of signal $s(t)$ by the in-phase and quadrature reference signal $p_f(t) = sin(2\pi ft + \varphi_r)$ and $q_f(t) = cos(2\pi ft + \varphi_r)$ and then on separate summation of these in SP_f and SQ_f:

$$SP_f = \sum_{i=1}^{N} T_{exp}(t_i)p_f(t_i); SQ_f = \sum_{i=1}^{N} T_{exp}(t_i)q_f(t_i) \tag{3}$$

$$T_1 = \frac{2}{N}\sqrt{SP_f^2 + SQ_f^2} \tag{4}$$

where, N is number of images per lock-in period (lock-in period is taken as one fatigue cycle), t_i is sampling interval which is $0.05sec$, since the acquisition frame rate is 20Hz, p_f and q_f are in-phase, $\sin(\omega t)$, and in-quadrature, $\cos(\omega t)$, lock-in correlation functions, respectively.

In order to monitor the evaluation of temperature at bending root, two tests were performed under force and displacement controlled conditions. During the force controlled test (F= 40kN) the evolution of temperature was monitored continuously. Fig. 3(a) shows the variation of temperature range versus numbers of cycles to failure in a logarithmic scale for the force controlled test. The data were extracted at nine points in the middle of bending area as depicted in Fig. 3(b). From Fig. 3(a) it can be noticed that the temperature ranges drop around 12×10^3 cycles. These temperature drops can be related to multiple micro cracks initiation onset. These interesting results reveal that the fatigue crack initiation lifetime is about 55% of total lifetime. Three distinguishable behaviours can be detected from logarithmic scale figure. It can be understood that, the temperature range of the surface rises non-linearly in the

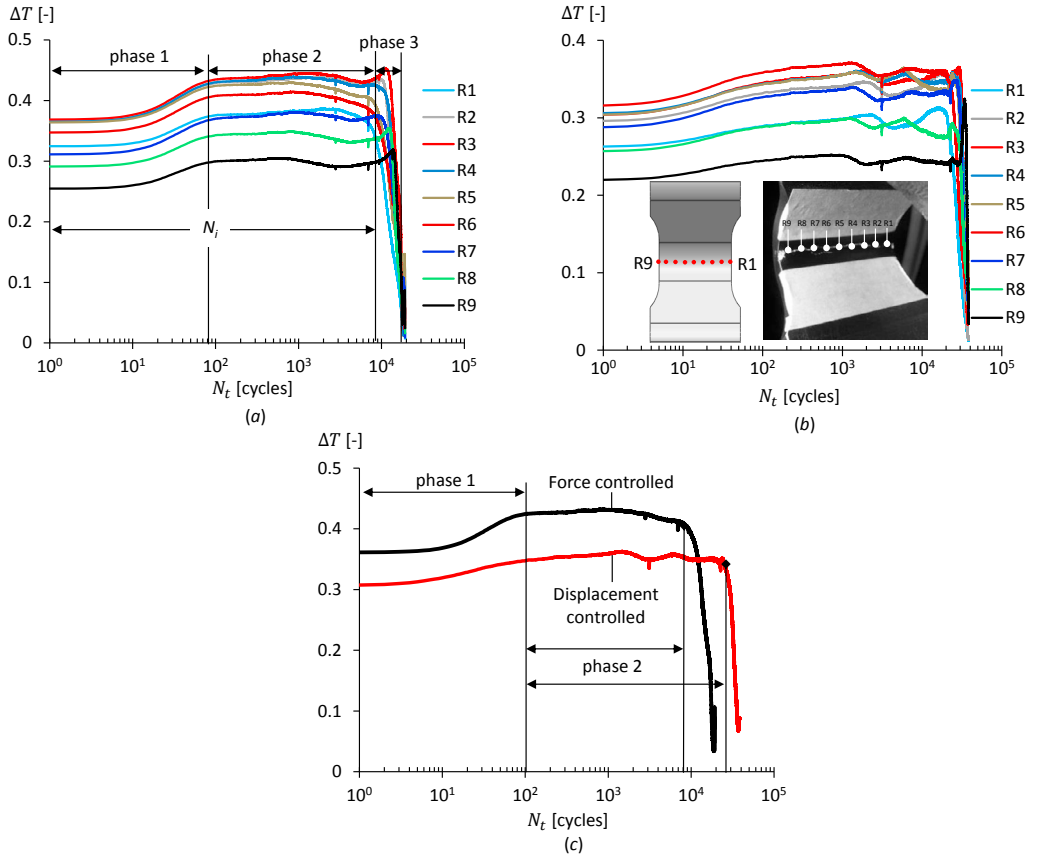

Fig. 3. variation of temperature range versus fatigue cycles to failure for (a) force and (b) displacement controlled experiments; (c) comparison of temperature range variation versus fatigue number of cycles between force and displacement control tests.

initial phase (phase 1), then reaches a stabilized asymptotic value (phase 2), and eventually this asymptote is left with a significant temperature range drop leading soon to failure after few cycles (phase 3). Thus, the first two phases are crack initiation step and the last phase is governed by crack propagation step.

To check the consistency of proposed approach and obtained results for detecting the onset of crack initiation, another test was performed under displacement control conditions using IR camera. The maximum axial displacement was applied based on the measured maximum displacement after stabilization point for load controlled fatigue test with a displacement ratio of 0.1. Fig. 3(b) shows the temperature range variation along the fatigue cycles to failure for displacement control test. The same behaviour as load controlled test can be observed for displacement control test. Fig. 3(c) compares the variation of temperature range versus the fatigue cycles between force and displacement control tests. The temperature ranges were averaged in the middle of the bending area of fatigue specimen i.e. from R3 to R6. As expected for displacement controlled test the fatigue lifetime is higher due to the fact that the global axial load decreases during fatigue cycling. For both tests the temperature range rises non-linearly up to 100 cycles and stabilizes after that. Moreover, the fatigue crack initiation lifetimes are around 55% and 64% of total lifetimes for load and displacement control tests respectively. The exact reason for this temperature-range decrease phenomenon has not been understood yet. One possibility could be the decrease of the thermal expansion coefficient due to the accumulation of voids inside the fatigue specimen. The void is the free space created between atoms. Due to the void accumulation process during fatigue, the total-volume increase of the material under the temperature increase will be less because the atoms will consume the free space inside the material first, which declines the thermal-expansion coefficient of the material, as suggested by Crupi et al. (2010).

4. Finite element analysis

In order to understand the effect of bending process on fatigue behaviour of different steel grades it is important to obtain more information about the multiaxial strain and stress states at and near the bending root after bending process and applied axial fatigue load. To do so, numerical technique approach was used to model the bending and spring back processes along with the fatigue loading.

Fig. 4(a) and (b) illustrates the finite element mesh, loading and boundary conditions that were used in this study for modelling the bending and spring back processes along with fatigue loading. As indicated in Fig. 4(a) for modelling the bending and spring back effect a 3D model was used, which consists of three parts, namely the bending specimen, punch and die. Fig. 4(b) shows the fatigue model including just the fatigue sample. Due to double symmetry configuration of experimental tests just one quarter of the fatigue specimen was modelled. 3D structural 8-node linear brick, reduced integration, hourglass control (C3D8R) elements were used with a master-slave contact algorithm on the contact surface between the sample, punch and die interfaces. As the vicinity of the bending area was the critical zone to be analysed, density of the mesh was appropriately refined in this region as shown in Fig. 4(b). The minimum mesh size around the bending area was 0.6mm and increased gradually far from the area of interest.

A finite sliding contact condition was used between the contact pair to transfer loads between the connected bodies. The contact surfaces were defined as a contact pair that enabled ABAQUS to determine if the contact pair was touching or separated. The penalty of friction was included in the contact pair to define the friction behaviour of the contact region (tangential behaviour) along with hard contact algorithm to model normal behaviour of contact. The coefficient of friction μ= 0.5 was considered in this study for steel to steel contact as lubrication was not used for the bending process. For both simulation steps material was modelled using isotropic hardening with yield stress-strain curve obtained from uniaxial tensile tests.

To simulate the bending process, the punch was pressed against the bending sample into the v-shaped die as illustrated in Fig. 4(a). The punch displacement was around 34.4mm, which was measured experimentally. The punch was moved up to relax the specimen for modelling the spring back effect. In order to avoid rigid body motions problem both sides of the specimen were fixed during the relaxation step. In fact by fixing both sides of the bending sample, the stress distribution represents the effect of clamping before applying the axial fatigue load. In order to model the fatigue loading conditions, the deformed mesh after relaxation (spring back) step was imported as an orphan mesh to a new model. It is worth to mention that the deformed geometry was validated against the experimental observations as is elaborated later on in this section. In addition, it was observed experimentally that the bending process induces compressive residual stresses. These residual stresses are relaxed after stabilization point under low cycle fatigue

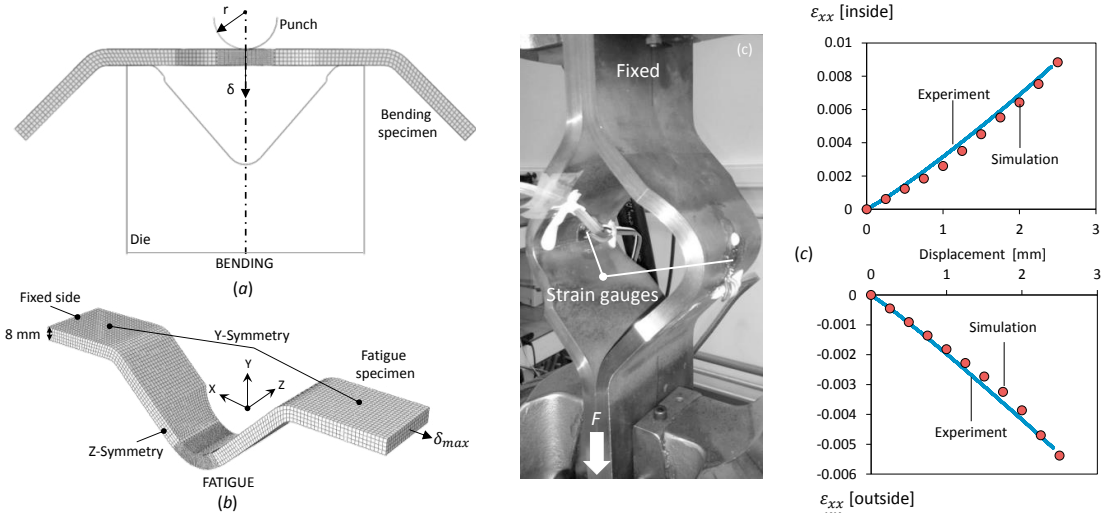

Fig. 4. Finite element mesh, loading and boundary conditions of (a) the bending and (b) the fatigue model; (c) comparison of the engineering strains and load versus displacement between numerical simulation and experimental observation at F= 40kN.

loading conditions. To this end, the mesh was imported into the model without any residual stress profile from the bending process. To model the fatigue loading conditions, instead of maximum axial load, the maximum displacement after the stabilization point was applied which was measured experimentally for each loading level.

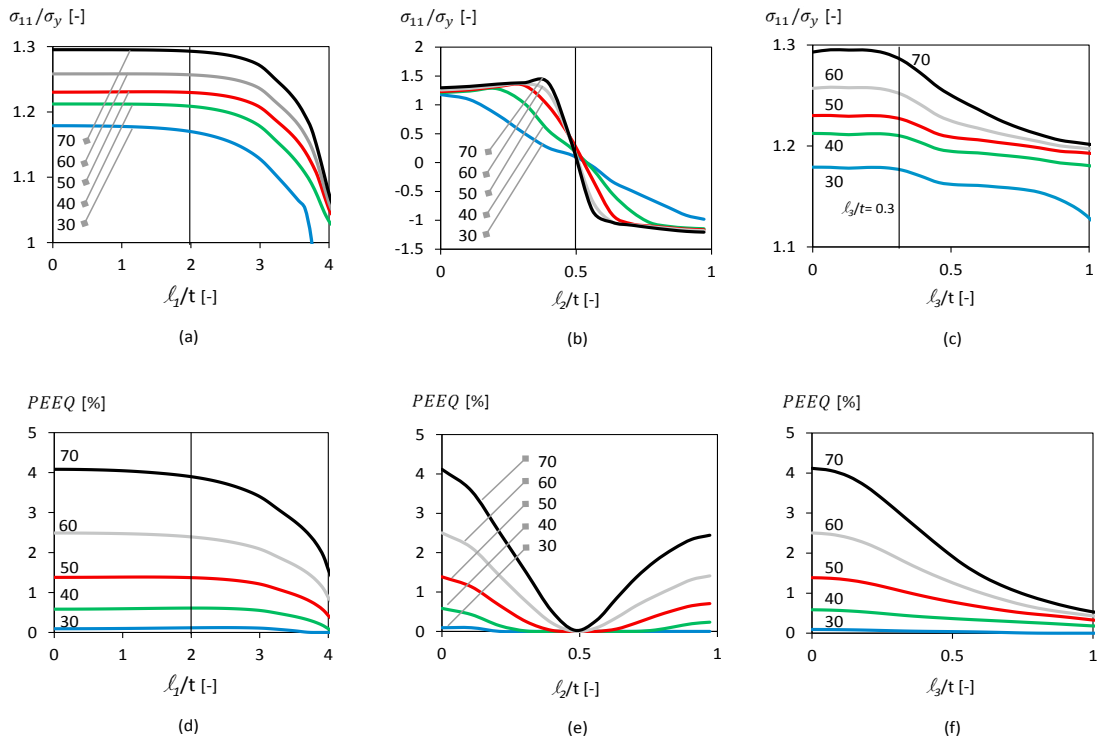

Fig. 5. Distribution of normalized maximum principal stress (σ_{11}) and equivalent plastic strain (PEEQ) along the (a and d) path 1 (l_1), (b and e) path 2 (l_2) and (c and f) path 3 (l_3) respectively. Paths are normalized with respect to the specimen thickness.

Fig.4 (c) shows the quasi static experimental set-up that was used to validate the fatigue model. The maximum axial load of 40kN was applied in quasi-static mode. Two strain gauges were mounted inside and outside of the bending area to measure the strains along the axial loading direction. Fig.4 (c) demonstrates the comparison between the experimental data versus the finite element measurements. As it can be seen, both experimental measured strains are in good correlation with the calculated simulation results.

As mentioned above, it is clear that the stress gradients are high and multiaxial at/near the bending root. To obtain more information about these high stress gradients the maximum principal stress and equivalent plastic strain variation were monitored along three different paths in middle of the bending area of fatigue sample for all applied fatigue loads i.e. F= 30 to 70kN, as indicated in Fig. 5. Fig 5(a) to (f) indicate the distribution of normalized maximum principal stress and equivalent plastic strain along the normalized paths. The maximum principal stress (σ_{11}) and different paths were normalized using yield stress and thickness of fatigue sample respectively. The zero ratio distance is in the middle of the specimen and l_1, l_2 and l_3 are along RD, ND and TD respectively.

Fig. 5(a) presents that the variation of σ_{11} is almost constant up to l_1/t= 2 and decreases gradually till the edge of the fatigue sample for all applied axial loads. In contrast, Fig. 5(b) reveals that the variation of σ_{11} is significant through the thickness of specimen and shift from tensile to compressive at the middle of specimen thickness for all cases. The variation of σ_{11} is less significant along l_3 up to 0.3 times of the sample thickness as depicted in Fig. 5(c). Fig. 5(d) to (f) illustrate the variation of PEEQ value along normalized l_1, l_2 and l_3 paths. From the figures it can be noticed that the magnitude of PEEQ is changing from 30kN to 70kN considerably. Fig. 5(d) shows that, like the maximum principal stress, the variation of PEEQ is negligible up to l_1/t= 2 for all loading conditions. Interesting results in Fig. 5(e) exposes that there is no plastic deformation in the middle of specimen thickness for all cases. Furthermore, it can be noticed that by increasing the axial load the difference between plastic deformation inside and out side of the bending area rises slightly. Although the maximum value of PEEQ occurs on the surface of the bending area for all applied axial loads. Eventually, Fig. 5(f) suggests that the plastic deformation is high at the bending root (l_3/t= 0) and declines slightly and drastically for the low and high applied axial loads respectively.

5. Conclusions

The main objective of this research study was to investigate the effects of pre-bending process on low cycle fatigue behaviour of different steel grades. In the first step, a new test specimen has been designed to study the effect of pre-bending process on low cycle fatigue behaviour of HSS. An advanced lock-in thermography approach was used to separate crack initiation and propagation lifetimes. Fractography and Scanning Electron Microscopy (SEM) analyses were performed to study the fracture surface of the failed fatigue specimens after the bending process and the fatigue testing. In addition, a three dimensional finite element modelling approach was used to simulate the bending process and fatigue loading conditions. The developed model allows to monitor the multiaxial stress and strain states inside the bending area. According to observed experimental observations, it is possible to find the micro-crack initiation onset by monitoring the temperature range variation inside the bending area using infrared thermography. It has been shown that using finite element modelling approach provides extra information such as multiaxial stress gradient inside the bending area, which is not possible to be monitored using the experimental test.

References

Basquin, OH., 1910. The exponential law of endurance tests. In: Proc. ASTM 10(2), 625–630.

Beretta, S., Bernasconi, A., and Carboni M., 2009. Fatigue assessment of root failures in HSLA steel welded joints: A comparison among local approaches. International Journal of Fatigue 31(1), 102–110.

Chen, H., Grondin, GY. and Driver, RG., 2007. Characterization of fatigue properties of ASTM A709 high performance steel. Journal of Constructional Steel Research 63(6), 838–848.

Coffin Jr, L. Fo. 1953. A study of the effect of cyclic thermal stresses on a ductile metal. Knolls Atomic Power Lab.

Crupi, V., Chiofalo, G., and Guglielmino, E., 2010. Using infrared thermography in low-cycle fatigue studies of welded joints. Welding Journal 89(9), 195–200.

Krapez, JC., 1998. Compared performances of four algorithms used for modulation thermography. In: Proc. of the Eurotherm Seminar 60, 7–10.

Manson, S., 1953. Behavior of materials under conditions of thermal stress. National Advisory Committee for Aeronautics, TN 2933.

Wohler, A., 1871. Tests to determine the forces acting on railway carriage axles and the capacity of resistance of the axles 11, 199.